Original Research Article

Pseudocapacitive Behavior of Nb₂O₅-TNTs Nanocomposite for Lithium-ion Micro-batteries

M. Mohammadifar [a], A. Massoudi [b,*], N. Naderi [c], M. J. Eshraghi [c]

[a] MS, Department of Semiconductors, Materials and Energy Research Center (MERC), Meshkindasht, Alborz, Iran

[b] Assistant Professor, Department of Semiconductors, Materials and Energy Research Center (MERC), Meshkindasht, Alborz, Iran

[c] Associate Professor, Department of Semiconductors, Materials and Energy Research Center (MERC), Meshkindasht, Alborz, Iran

ARTICLE INFO

ABSTRACT

The present study aims to introduce Niobium pentoxide-Titanium nanotube (Nb_2O_5-TNTs) composite as a novel anode material synthesized through hydrothermal method. In this respect, Nb_2O_5 nanoparticles and TNTs are separately synthesized through sonochemical and anodizing processes, respectively. According to FESEM images, the well-oriented TNTs with inner and outer diameters of 70 and 88 nm, respectively, are well decorated by Nb_2O_5 nanoparticles. The Nb_2O_5-TNTs anode shows the areal charge and discharge capacities of 0.167 mAh/cm² and 0.146 mAh/cm², respectively, at 0.113 mA/cm² as well as 60% capacitive storage in 20 mV/s. High power Nb_2O_5-TNT anode reveals 86% reversible capacity in the 16th cycle with a columbic efficiency of 84% for the 16th cycle. In addition, the charge transfer resistance in TNTs declines from 750 Ω to 680 Ω after decorating by Nb_2O_5. The superior performance of Nb_2O_5-TNT composites is taken into account to derive higher charge storage from a capacitive charge storage which is dominant in the diffusion-controlled process. Therefore, Nb_2O_5-TNT composite can be applied to the next-generation pseudocapacitive anode in lithium-ion batteries.

1. INTRODUCTION

Ultrafast rechargeable lithium-ion batteries with a high charging rate, high energy density, and long life cycle are vastly used in portable electronics and microdevices. Both supercapacitor-like rate performance and battery-like capacity with a long lifetime are highly demanded in producing microsensors, smart medicine, small power sources, and so on [1-5]. One of the main advantages of lithium-ion micro-batteries is its thickness on a micrometer range and safety. They also enjoy several economic advantages such as their environmentally-friendly components, durable rechargeability, and their ability to be prepared in any shape or size of different substrates, to name a few [6,7].

Nonetheless, common lithium-ion batteries suffer from sluggish ion transfer which result in low kinetics. To provide a fast Li-ion reaction and diminish sluggish ion transfer, intercalation compounds with robust structure with open channels and the intercalation pseudocapacitance materials are the best candidates [8,9]. Till now, numerous researches have demonstrated that metal oxides with both stable structures and multicharge careers can be a good choice for lithium-ion insertion and extraction in and from the anode and cathode material. These materials with high-rate capabilities and rational designs lead to the enhancement

---

of the diffusion of Li-ions into the electrode depth and improvement of the kinetics to achieve the maximum ion/electron transfer rate [10-15]. Indeed, the high-rate capability of lithium-ion batteries is limited due to random ion movement resulting from the low kinetics of redox reactions. Therefore, capacitive and pseudocapacitive materials can improve kinetics because the corresponding reduction and oxidation are surface-controlled [16,17].

As a new type of capacitance, pseudocapacitance is equal to derivation $d(\Delta q)/d(\Delta E)$ which is faradaic in nature. An important difference between pseudocapacitance and battery-like behavior is a change in the chemical reactant resulting from the faradaic charge transfer of the surface. There are three different types of capacitive charge storage mechanisms: adsorption, redox, and intercalation. Adsorption capacitance contains adsorption and desorption on metallic atom surfaces. Unlike adsorption pseudocapacitance, redox pseudocapacitance contains faradaic redox reactions on the electrode surface. While the charge is stored through surface coverage in adsorption, it is stored through chemical conversion between oxidation and reduction species on the surface in redox. This behavior is pseudocapacitive in nature because lithium ions are accommodated faradically in quasi two-dimensional planes in van der waals gap of the layer structure of the host material [18-21].

In this regard, one of the materials that can be applied in high-energy lithium-ion micro-batteries is Titania (TiO_2) which is a promised 3D intercalative material with the prior mechanical and chemical stability in the electrolyte window potential. Insertion and extraction of Li-ions in and from the TiO_2 structure mainly occur at 1.5 V versus Li/Li^+, while the $LiPF_6$ electrolyte compound reduces at 0.6-1 V versus Li/Li^+. Consequently, this phenomenon causes electrochemical stability of TiO_2 [22, 23]. Until now, many nanostructures of TiO_2 are used in lithium-ion batteries such as 3D microstructures, nanowires, nanotubes, nanorods, and nanoparticles. Among them, nanotube is the best structure due to the highest surface areas among other nanostructures [24,25]. In addition, the outer and inner walls of the tube make more active sites intercalate Li-ions into the TiO_2 lattice structure to form Li_xTiO_2 ($0<x<1$) [26]. Titania introduces the theoretical surface capacity of 125 mAh/cm^2. In 2009, F. Ortiz et al. prepared self-organized TiO_2 nanotubes with a maximum charge and discharge areal capacity of 77 $\mu Ah/cm^2$ with retention up to 90% over 50 cycles [27]. In 2011, Wei Wang et al. synthesized three-dimensional Ni/TiO_2 nanowire on the Ni foil with 0.016 mAh/cm^2 at 12 C with 20 cycles stability [28].

Furthermore, titanium niobium binary metal oxides, such as $TiNb_2O_7$ and $Ti_2Nb_{10}O_{29}$, seem to be interesting candidates for high-rate performances. Since $T-Nb_2O_5$ offers 2D transport pathways and little change in the lattice volume after lithium-ion intercalation, it

guarantees original crystal structure maintenance [29-31]. Moreover, it enjoys the advantage of a pseudocapacitive charging mechanism. Recently, Lubke et al. illustrated that Nb dopant in TiO_2 nanofiber could improve the rate capability due to its high electrical conductivity and low lithium-ion diffusion paths resulting from a decrease in the crystallite size. The average capacities after 20 cycles in 5 C rate for doped and non-doped TiO_2 were 23 and 10 mAh/cm^2, respectively [32]. The present study considered decorating TNTs by $T-Nb_2O_5$ nanoparticles in order to prepare an innovative Nb_2O_5-TNT composite for the first time to construct a pseudocapacitive lithium-ion battery.

In this study, TNTs as an intercalative anode was synthesized through fluorinated electrolyte anodization. Moreover, Nb_2O_5 nanoparticles were synthesized through the surfactant-free sonochemical method and were decorated on TNTs through the hydrothermal method. The rate capability of samples was confirmed. Moreover, the pseudocapacitive behavior of the prepared electrode was investigated using the ratio of diffusion-controlled to surface-controlled contributions in cyclic voltammograms.

2. MATERIALS AND METHODS

2.1. Anodization of TiO₂ Nanotubes

First, Titanium sheets (99.7% purity) were mechanically polished and cleaned with ethanol (99%, Merck) and deionized water. For setting up, Titanium sheet was used as an anode and pure platinum (Pt) mesh as a cathode. Electrolyte solution was prepared using 1 wt% hydrofluoric acid (HF, 28%, Merck). Anodization was performed in a constant voltage condition of 20 V for 20 min. Finally, the samples were rinsed with deionized water and dried with N_2. To crystallize titanium nanotubes (TNTs), the samples were calcinated at 300 °C for 1 h.

2.2. Sonochemical Synthesis of Nb₂O₅ Nanoparticle

Synthesis of Nb_2O_5 nanoparticles using ultrasonic bath has been previously reported in the literature [33]. To be specific, commercial Nb_2O_5 powder was dissolved in HF and stirred at 100 °C for 1 h. The solution was diluted to the concentration of 2 g/L. After one hour of ultrasonication, the pH of the solution was adjusted to 9 using ammonia. Then, the final product was leached with EtOH and DI water and dried at 85 °C for 6 h to obtain amorphous Nb_2O_5. Finally, the white powder was calcined at 880 °C for 30 min at a heating rate of 10 °C/min.

2.3. Nb₂O₅-TNTs Composite Preparation

Nb_2O_5 nanoparticles were decorated on TNTs by hydrothermal treatment. The Nb_2O_5 decoration solution

served in a Teflon-lined stainless steel autoclave with different concentrations of Nb_2O_5 nanoparticles dispersed into the deionized water. The TNT sheet is supported as a substrate. The samples were hydrothermally treated at 85 °C for 9 h. Then, after washing them with deionized water and annealing at 400 °C for 2 h at a heating rate of 10 °C/min, the Nb_2O_5-TNTs was formed.

2.4. Material Characterization

X-Ray Diffraction (XRD) analysis of the samples was carried out using Philips (PW 3710) X-ray diffractometer with graphite monochromatized Co kα radiation (λ= 1.78901 Å) in the angle range of 5 to 85 degrees with a step of 0.02 degrees per minute. In addition, Field Emission Scanning Electron Microscopy (FESEM) equipped with energy-dispersive X-ray spectroscopy was carried out using Mira 3-XMU. The FT-IR spectra were measured by Pekin-Elmer (spectrum 400).

2.5. Electrode Fabrication and Electrochemical Measurement

The electrochemical performance of the synthesized TNTs and Nb_2O_5-TNTs was evaluated by the half-cell design in a coin cell. Two electrodes of electrochemical cells were constructed in an Ar-filled glovebox. The TNTs on Ti sheet and Nb_2O_5-TNTs composite (binder-free and carbon-free) were used as the working electrode with the lithium metal foil used as both reference and counter electrodes. The electrolyte utilized 1M $LiPF_6$ in EC: DMC in 1:1 vol.%. Charge-discharge tests and cyclic voltammetry were carried out through galvanostat/potentiostat (PGS 2065). The current densities from 0.019 mA/cm^2 to 0.565 mA/cm^2 with the cutoff voltage of 3.5 V vs. Li/Li$^+$ are selected for charge-discharge. The scan rates of 0.5, 1, 3, 5, 7, 10, and 20 mV/s were applied for the cyclic voltammetry test. Electrochemical Impedance Spectroscopy (EIS) was applied over the frequency range of 1 MHz to 1 mHz with 2 V amplitude AC voltage by EG & G (parstat 2273, USA).

In order to calculate the size of a specific surface area of an anode, TNTs were assumed as a perfect cylinder according to the Ortiz approach [27]. Following the approximation of a number of nanotubes, the measured area of every nanotube through the 2π(R-r)*h formula is multiplied by the number of nanotubes. In this method, R is the outer radius, r the inner radius, and h the height of each cylinder (nanotube).

3. RESULTS AND DISCUSSION

3.1. Structural Characterization

Fig. 1a shows the XRD pattern of TNTs with the main high-intensity peak of (101) observed at 25°. The crystal structure of TNTs is tetragonal with l41/amd space

group, lattice parameters of a=3.78 Å and c=9.5 Å, and cell volume of 136.25 Å^3. The average crystallite size for (101) direction of TNTs is calculated through the Sherrer formula [32] as 27 nm with 0.62% lattice strain. The six other peaks of Ti are related to the substrate of TNTs in the anodizing method. The crystal structure of titanium is hexagonal with the P63/mmc space group and cell volume of 35.30 Å^3. Fig. 1b shows the XRD pattern of Nb_2O_5 nanoparticles at 880 °C, corresponding to the orthorhombic crystallite phase (T-Nb_2O_5). The average crystallite size is calculated by 80 nm with a strain lattice of 0.14%. In addition, the large ratio of c/a and huge volume lattice are the main parameters for easy movement of Li$^+$ into lattice through open channels, which are measured as 0.64 Å and 711.6 Å^3, respectively, for T-Nb_2O_5.
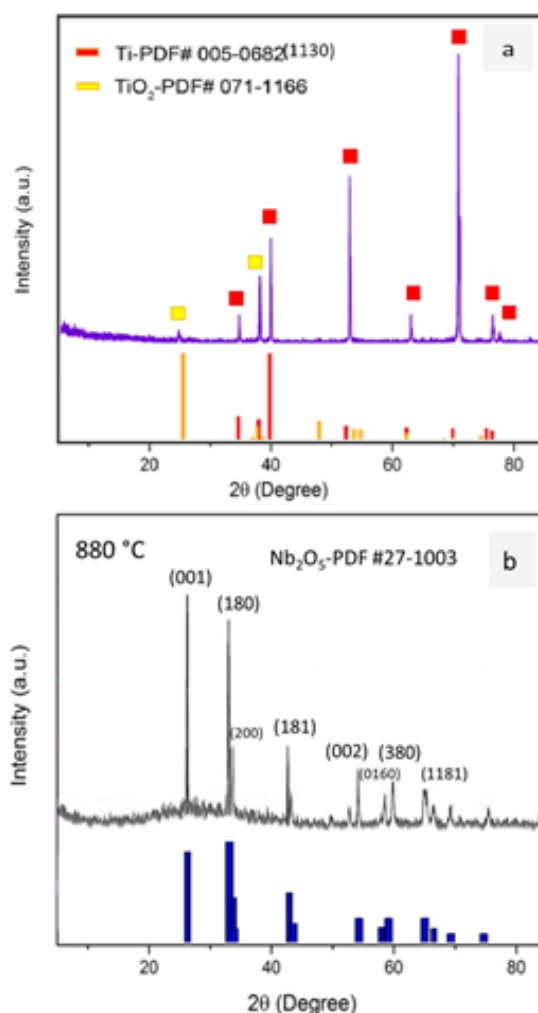

Figure 1. X-ray diffraction analysis of a) TNTs via anodizing method and b) Nb_2O_5 at 880 °C

Fig. 2a shows the homogeneity morphology of the synthesized titania nanotubes using the electrochemical anodization at 20 V. In the anodization process, first, an oxidant layer is formed on the titanium substrate. Then,

some pores and pits are formed on the oxidant layer, thus leading to the formation of nanotubes [34]. As seen in Fig. 2b, TNTs with the average inner and outer diameters of 70 and 88 nm, respectively, are well-oriented without any breakage. The synthesized Nb_2O_5 nanoparticles possess an average diameter of 41 ± 10 nm which was already reported in the literature [33]. To the best of the author's knowledge, ultrasonic energy forms pressure cycles and increases pressure locally whether the temperature remains constant or not; consequently, liquid water is transformed to steam and cavitation happens. Then, cavitation produces a strong shear force called jet liquid. Therefore, nucleation follows a different route, and nuclei are broken into smaller ones [35,36]. Fig. 2d demonstrates the TNTs decorated by Nb_2O_5 nanoparticles (NPs) which are decorated among the walls. In addition, there are some NP clusters on the top surface of the TNTs. A wide dispersion of all Ti, Nb, and O elements on the TNT surface, as shown in Fig. 2e, illustrates an interesting decoration among walls. Moreover, weight percentages of 0.36, 70.88, and 28.75 for Ti, Nb, and O, respectively, confirm the presence of Nb_2O_5 decorated on TNTs with no sign of impurity and contaminant.
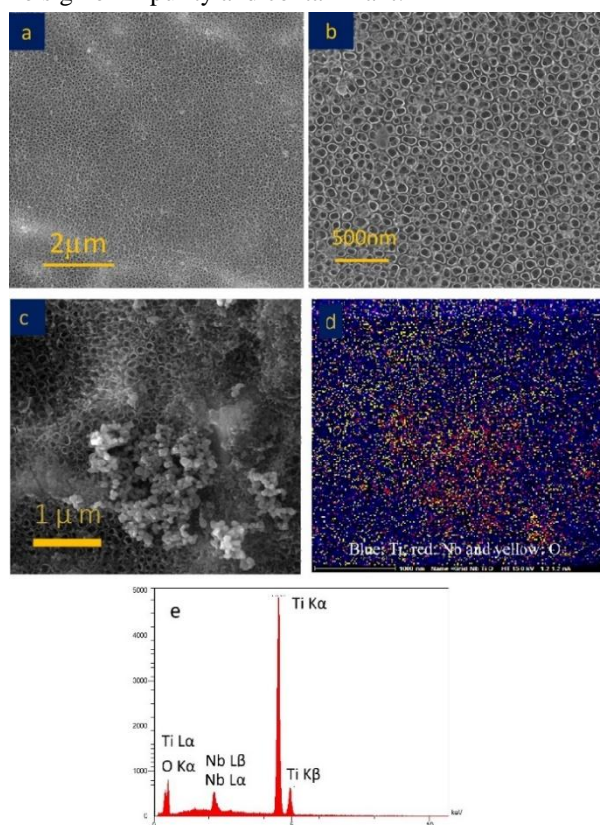

Figure 2. The FESEM images of a, b) TNTs in two different magnifications, c) Nb_2O_5-TNTs composite synthesized through hydrothermal and calcined at 400 °C, d) EDS map of the Nb_2O_5-TNTs composite, and e) EDS spectra of the Nb_2O_5-TNTs composite

3.2. Electrochemical Performance

Figs. 3a and 3c show the cyclic voltammetry of TNTs at the scan rate of 1 mV/s. According to Equation 1, an anodic peak at 2.16 V corresponds to the oxidation of Li^+ from the lattice of TNTs, and the reduction peak at 1.66 V is observed during the lithiation process.

$$xLi^+ + xe^- + TiO_2 \leftrightarrow Li_xTiO_2 \tag{1}$$

Moreover, the electrochemical behavior of Nb_2O_5-TNT anode was investigated through the cyclic voltammetry at the same scan rate. As observed in Figs. 3b and 3d, the electrochemical activity of $Nb^{+5} \leftrightarrow Nb^{+3}$ during oxidation and reduction of Li^+ ion into the Nb_2O_5 structure, according to Equation 2, occurs between 1.25 and 2.25 V.

$$xLi^+ + xe^- + Nb_2O_5 \leftrightarrow Li_xNb_2O_5 \tag{2}$$

This peak is not sharp, thus indicating the intercalation and surface energy storage. It is also indicative of the amorphous shape, low crystallinity, and low electrolyte conduction.

3.2.1. Investigation of Pseudocapacitive Behavior of TNTs and Nb_2O_5-TNTs Anodes

To investigate the pseudocapacitive behavior, separating diffusion-controlled and surface-controlled contributions of lithium storage in TNTs and Nb_2O_5-TNTs, cyclic voltammograms are taken at different scan rates. The relation between current (i) and scan rate (v) is elaborated through Equation 3, where a and b are the constant coefficients. The value of b varies from 0.5 to 1. In case b is 0.5, the lithium storage is completely diffusion-controlled and if it is 1, the lithium storage is totally capacitive-controlled. In the middle values between 0.5 and 1, both contributions of diffusion and surface storage are implied [37].

$$i = av^b \tag{3}$$

The b value is derived from the slope of the plot of ln i-ln v, derived from CV curves in Figs. 3a and 3b, according to Equation 4.

$$\ln i = b \ln v + \ln a \tag{4}$$

Figs. 4a and 4b depict the slope of ln i-ln v by cyclic voltammetry in both oxidation and reduction states for TNTs, respectively. The slope parameters for oxidation and reduction are calculated as 0.66 and 0.63, respectively. Since this value is between 0.5 and 1, it has both diffusion-controlled and surface-controlled contributions.
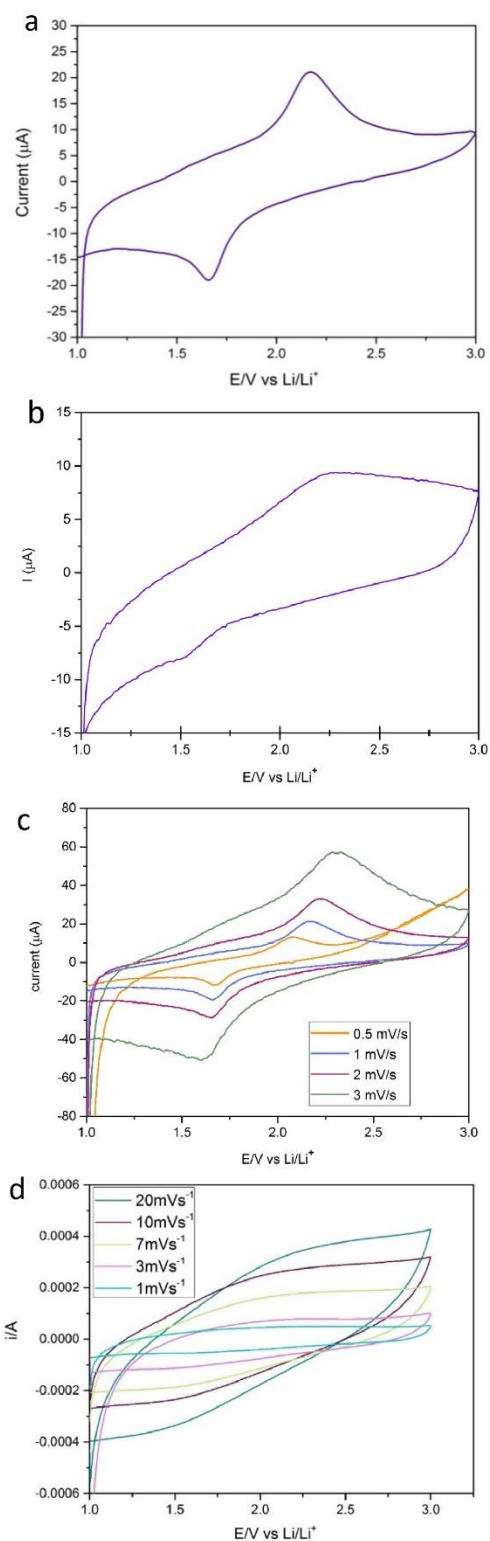
Figure 3. Cyclic voltammetry of a) TNTs in 1 mV/s, b) Nb_2O_5 in 1 mV/s, c) cyclic voltammetry of TNTs in 0.5, 1, 2 and, 3 mV/s, and d) cyclic voltammetry for Nb_2O_5-TNTs electrode in 1, 3, 7, 10, and 20 mV/s
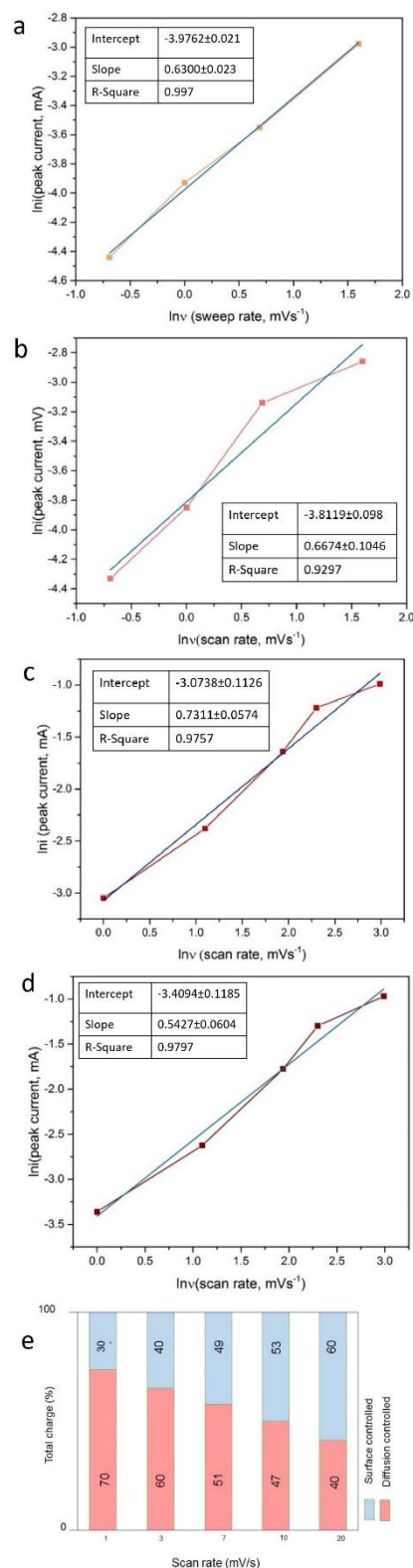
Figure 4. a) lni-lnv in TNTs oxidation, b) lni-lnv in TNTs reduction, C) lni-lnv in Nb_2O_5-TNTs oxidation, d) lni-lnv in Nb_2O_5-TNTs reduction, and e) surface to diffusion contribution in lithium-ion storage in Nb_2O_5-TNTs composites

Moreover, Figs. 4c and 4d show the slopes of ln i-ln ν for Nb_2O_5-TNTs anode in terms of defining capacitive and diffusive control contributions in oxidation and reduction procedures. The slope values for oxidation and reduction are 0.84 and 0.73, respectively, between 0.5 (diffusion-controlled) and 1 (surface-controlled). Therefore, they have both capacitive and diffusion-controlled contributions [38]. A comparison of these values in TNTs and Nb_2O_5-TNTs shows that b_{Nb-Ti} > b_{TNTs}. This inequality is true in oxidation and reduction procedures. Therefore, capacitive contribution in Nb_2O_5-TNTs anode is more than that in TNTs anode since as expected, Nb_2O_5-TNTs anode has better pseudocapacitive storage than TNTs anode.

The restricted area by CV is indicative of the surface charge storage contribution (pseudocapacitance and double layer) and diffusion-controlled process (lithium intercalation). Upon increasing the scan rate, cyclic voltammetry area would increase due to more lithium-ion storage, hence higher charge storage at higher rates. The Nb_2O_5-TNTs electrode can store energy in surface reaction. In order to separate capacitive and diffusion-controlled contributions, the peak current in CV is plotted versus ν and $ν^{1/2}$, according to Equation 5, where $k_1ν$ denotes capacitive storage due to fast kinetics and $k_2ν^{1/2}$ presents the diffusion-controlled terms due to sluggish kinetics [8,11,32].

$$i_g = k_1ν + k_2ν^{1/2} \qquad (5)$$

As shown in Fig. 4e, the ratio of surface to diffusion contribution increases upon increasing the scan rate from 1 mV/s to 20 mV/s in the Nb_2O_5-TNTs composite anode. As a result, the surface storage increases from 30% to 60% of the total charge storage at high sweep rates that mean more pseudocapacitive behavior and less intercalative behavior.

3.2.2. Charge and Discharge Performance

Fig. 5a shows the areal capacity of TNTs at 0.019 mA/cm². The initial charge and discharge capacities are 0.045 mAh/cm² and 0.018 mAh/cm², respectively. The second charge and discharge capacities are reduced to 0.026 mAh/cm² and 0.028 mAh/cm², respectively, due to the SEI layer formation on the electrode-electrolyte interface. The lithiation and de-lithiation plateaus at around 1.5-2 and 2-2.5 V are in agreement with the cyclic voltammogram of TNTs. The initial, second, and third charge capacities at 0.097 mA/cm², as can be seen in Fig 5b, are 0.009 mAh/cm², 0.015 mAh/cm², and 0.0137 mAh/cm², respectively, and the initial, second, and third discharge capacities are 0.0125 mAh/cm², 0.0138 mAh/cm², and 0.0195 mAh/cm², respectively.

Fig. 5c shows the areal capacity of Nb_2O_5-TNTs at 0.113 mA/cm². The first charge and discharge capacities are 0.412 mAh/cm² and 0.209 mAh/cm², respectively.
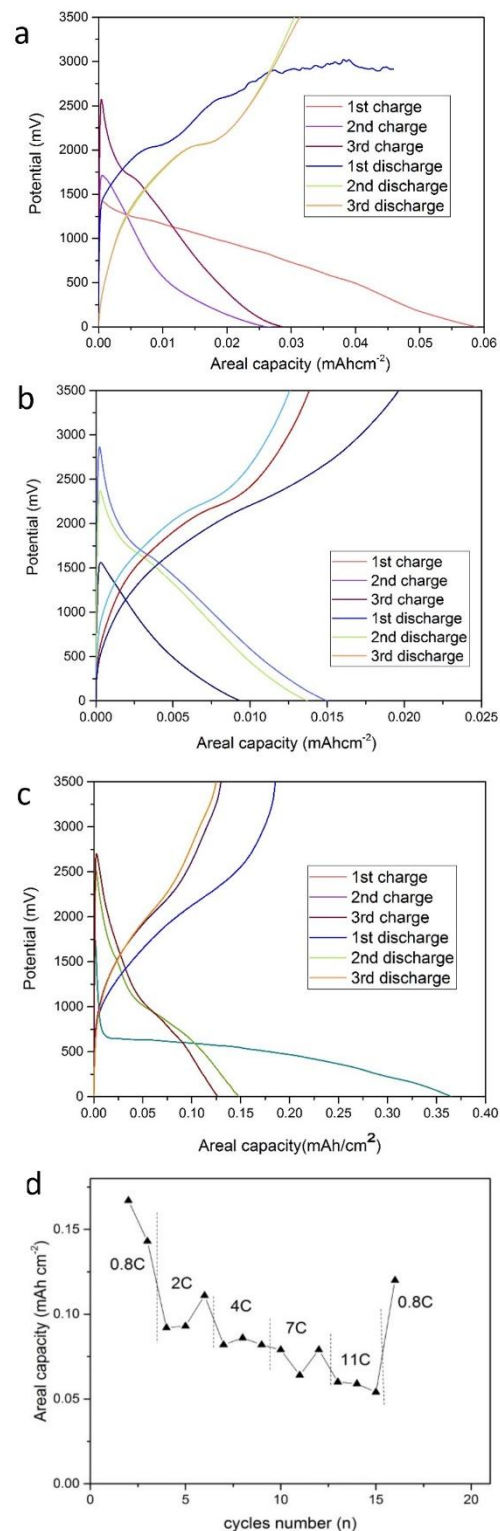

Figure 5. a) Initial, second, and third charges and discharges of TNTs anode at 0.019 mA/cm², b) Initial, second, and third charges and discharges of TNTs anode at 0.097 mA/cm², c) Initial, second, and third charges and discharges of Nb_2O_5-TNTs anode at 0.113 mA/cm², and d) Rate capability of Nb_2O_5-TNTs anode at different rates of 0.8 C, 2 C, 4 C, 7 C, and 11 C

The second charge and discharge capacities are reduced by 0.167 mAh/cm^2 and 0.146 mAh/cm^2, respectively, owing to the formation of a stable SEI. Like the TNTs anode, the plateaus of lithiation and de-lithiation are 0.5-1.5 V and 2-2.5 V being in line with cyclic voltammetry for Nb$_2$O$_5$-TNTs composite.

Fig. 5d shows the rate capability of Nb$_2$O$_5$-TNTs anode for 16 cycles at different rates. As can be seen, the areal capacity is reduced from 0.16 mAh/cm^2 at 0.8 C to 0.09 mAh/cm^2 at 2C, to 0.08 mAh/cm^2 at 4 C, and to approximately 0.06 mAh/cm^2 at 11 C. Of note, 1 C is equal to full-lithiation of a bulk material during one hour. Nonetheless, when the applied current turns back to 0.8 C, the areal capacity of 0.12 mAh/cm^2 is recovered. Furthermore, coulombic efficiency in the 16th cycle is measured around 86% which is an indicator of structural stability of Nb$_2$O$_5$-TNTs electrode at high current rates.

3.2.3. Electrochemical Impedance Spectroscopy

The EIS experiments are evaluated after 20 cycles at the state discharge of 50 %. The Nyquist curves of TNTs and Nb$_2$O$_5$-TNTs and corresponding equivalent circuits are plotted in Fig. 6. The equivalent circuit for both TNTs and Nb$_2$O$_5$-TNTs consists of electrolyte resistance (Rs), constant phase element, charge transfer resistance (Rp), and Warburg impedance. Rs is measured to be 21 Ω for TNTs and 24 Ω for Nb$_2$O$_5$-TNTs. Differences in ohmic resistances are caused by separator and series connections. Moreover, Rp is calculated to be 680 Ω for Nb$_2$O$_5$-TNTs and 750 Ω for TNTs. Decrement of charge transfer resistance in Nb$_2$O$_5$-TNTs anode is due to pseudocapacitance charge storage. Furthermore, Warburg impedance is equal to 470 Ω for Nb$_2$O$_5$-TNT and 3400 Ω for TNTs. Increment of Warburg impedance in TNTs is followed by intercalation diffusion of lithium-ion in lattice structure, whereas in Nb$_2$O$_5$-TNTs, the mechanism is surface-controlled.
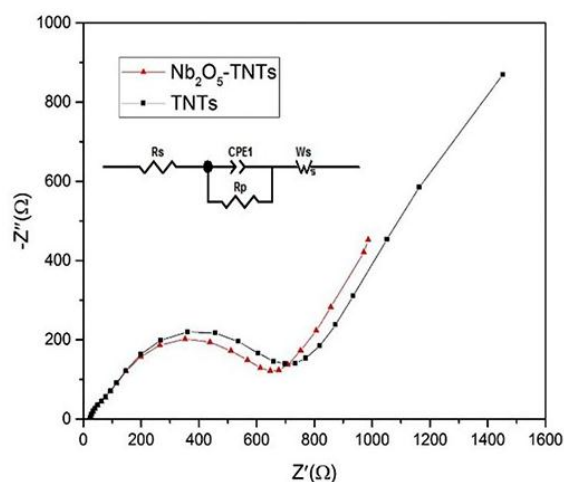

Figure 6. The Nyquist spectra with an equivalent circuit of TNTs and Nb$_2$O$_5$

Fig 7. shows the surface of the Nb$_2$O$_5$-TNT composite after cycling. As can be seen, the surface of the electrode is covered by Solid-Electrolyte Interface (SEI). Moreover, the Nb$_2$O$_5$ nanoparticles are swelled due to surface capacitance. In addition, core of each TNT is filled by lithium compounds during Li$^+$-ion intercalation.
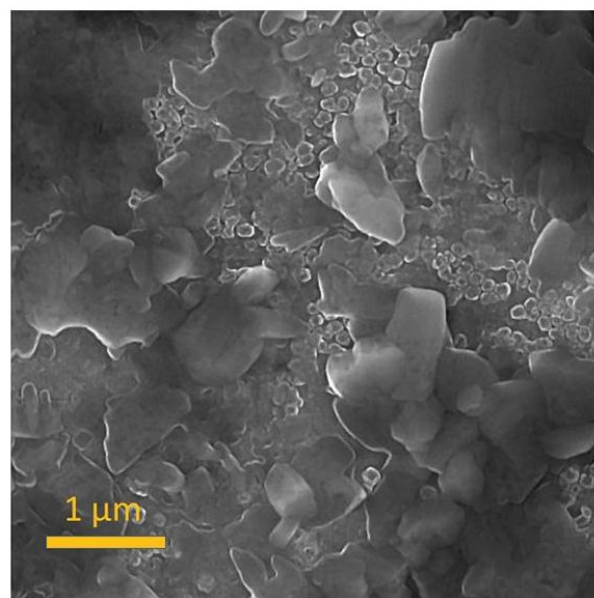

Figure 7. The surface characterization of the Nb$_2$O$_5$-TNT anode after cycling.

4. CONCLUSION

In summary, Nb$_2$O$_5$ nanoparticles were synthesized by sonochemical method and the average diameter of 41 nm to obtain desirable pseudocapacitive characteristics. Titania nanotubes with an external radius of 88 nm were successfully synthesized using the anodization process at 20 V. The Nb$_2$O$_5$ nanoparticles were decorated on titania nanotubes via hydrothermal method. The electrochemical characteristics of Nb$_2$O$_5$-TNTs and TNTs were analyzed by cyclic voltammetry, galvanostatic charge/discharge tests, and EIS. The CV curve of titania nanotubes showed oxidation and reduction peaks at 2.16 and 1.66 V, respectively, being inconsistent with titania nanotubes studies. The CV curve of Nb$_2$O$_5$-TNTs anode revealed pseudocapacitive behavior with 60% capacitive storage at 20 mV/s. The initial charge and discharge areal capacities of TNTs at 0.019 mA/cm^2 were reported 0.045 mAh/cm^2 and 0.018 mAh/cm^2, while the Nb$_2$O$_5$-TNTs composite showed the areal charge and discharge capacities of 0.167 mAh/cm^2 and 0.146 mAh/cm^2 at 0.113 mA/cm^2. Moreover, the charge transfer resistance in TNTs declined from 750 Ω to 680 Ω upon decoration by Nb$_2$O$_5$.

ACKNOWLEDGEMENT

REFERENCES

1. Nitta, N., Wu, F., Lee, J. T., Yushin, G., "Li-ion battery materials: present and future", *Materials Today*, Vol. 18, No. 5, (2015), 252-264. https://doi.org/10.1016/j.mattod.2014.10.040

2. Ning, H., Pikul, J. H., Zhang, R., Li, X., Xu, S., Wang, J., Rogers, J. A., King, W. P., Braun, P. V., "Holographic patterning of high-performance on-chip 3D lithium-ion microbatteries", *Proceedings of the National Academy of Sciences*, Vol. 112, No. 21, (2015), 6573-6578. https://doi.org/10.1073/pnas.1423889112

3. Goriparti, S., Miele, E., De Angelis, F., Di Fabrizio, E., Zaccaria, R. P., Capiglia, C., "Review on recent progress of nanostructured anode materials for Li-ion batteries", *Journal of Power Sources*, Vol. 257, (2014), 421-443. https://doi.org/10.1016/j.jpowsour.2013.11.103

4. Oudenhoven, J. F., Baggetto, L., Notten, P. H., "All-solid-state lithium-ion microbatteries: a review of various three-dimensional concepts", *Advanced Energy Materials*, Vol. 1, No. 1, (2011), 10-33. https://doi.org/10.1002/aenm.201000002

5. Feng, X., Li, Q., Wang, K., "Waste Plastic Triboelectric Nanogenerators Using Recycled Plastic Bags for Power Generation", *ACS Applied Materials and Interfaces*, Vol. 13, No. 1, (2021), 400-410. https://doi.org/10.1021/acsami.0c16489

6. Tang, Y., Zhang, Y., Li, W., Ma, B., Chen, X., "Rational material design for ultrafast rechargeable lithium-ion batteries", *Chemical Society Reviews*, Vol. 44, No. 17, (2015), 5926-5940. https://doi.org/10.1039/c4cs00442f

7. Kai, W., Xiao, F., Jinbo, P., Jun, R., Chongxiong, D., Liwei, L., "State of charge (SOC) estimation of lithium-ion battery based on adaptive square root unscented kalman filter", *International Journal of Electrochemical Science*, Vol. 15, No. 9, (2020), 9499-9516. https://doi.org/10.20964/2020.09.84

8. Augustyn, V., Simon, P., Dunn, B., "Pseudocapacitive oxide materials for high-rate electrochemical energy storage", *Energy and Environmental Science*, Vol. 7, No. 5, (2014), 1597-614. https://doi.org/10.1039/c3ee44164d

9. Griffith, K. J., Forse, A. C., Griffin, J. M., Grey, C. P., "High-Rate Intercalation without Nanostructuring in Metastable Nb_2O_5 Bronze Phases", *Journal of the American Chemical Society*, Vol. 138, No. 28, (2016), 8888-8899. https://doi.org/10.1021/jacs.6b04345

10. Augustyn, V., Come, J., Lowe, M. A., Kim, J. W., Taberna, P. L., Tolbert S. H, Abruña, H. D., Simon, P., Dunn, B., "High-rate electrochemical energy storage through Li+ intercalation pseudocapacitance", *Nature Materials*, Vol. 12, No. 6, (2013), 518-522. https://doi.org/10.1038/nmat3601

11. Brezesinski, K., Wang, J., Haetge, J., Reitz, C., Steinmueller, S. O., Tolbert, S. H., Smarsly, B. M., Dunn, B., Brezesinski, T., "Pseudocapacitive Contributions to Charge Storage in Highly Ordered Mesoporous Group V Transition Metal Oxides with Iso-Oriented Layered Nanocrystalline Domains", *Journal of the American Chemical Society*, Vol. 132, No. 20, (2010), 6982-6990. https://doi.org/10.1021/ja9106385

12. Zhao, Y., Gao, X., Gao, H., Jin, H., Goodenough, J. B., "Three Electron Reversible Redox Reaction in Sodium Vanadium Chromium Phosphate as a High-Energy-Density Cathode for Sodium-Ion Batteries", *Advanced Functional Materials*, Vol. 30, No. 10, (2020), 1908680. https://doi.org/10.1002/adfm.201908680

13. Zhao, Y., Gao, X., Gao, H., Dolocan, A., Goodenough, J. B., "Elevating Energy Density for Sodium-Ion Batteries through Multielectron Reactions", *Nano Letters*, Vol. 21, No. 5, (2021), 2281-2287. https://doi.org/10.1021/acs.nanolett.1c00100

14. Zhao, Y., Ding, C., Hao, Y., Zhai, X., Wang, C., Li, Y., Li, J., Jin, H., "Neat Design for the Structure of Electrode To Optimize the Lithium-Ion Battery Performance", *ACS Applied Materials and Interfaces*, Vol. 10, No. 32, (2018), 27106-27115. https://doi.org/10.1021/acsami.8b00873

15. Wang, C., Zhao, Y., Su, D., Ding, C., Wang, L., Yan, D., Li, J., Jin, H., "Synthesis of NiO Nano Octahedron Aggregates as High-Performance Anode Materials for Lithium Ion Batteries", *Electrochimica Acta*, Vol. 231, (2017), 272-278. https://doi.org/10.1016/j.electacta.2017.02.061

16. Guan, L., Yu, L., Chen, G. Z., "Capacitive and non-capacitive faradaic charge storage", *Electrochimica Acta*, Vol. 206, (2016), 464-478. https://doi.org/10.1016/j.electacta.2016.01.213

17. Wang, K., Liu, C., Sun, J., Zhao, K., Wang, L., Song, J., Duan, C., Li, L., "State of charge estimation of composite energy storage systems with supercapacitors and lithium batteries", *Complexity*, (2021), 2021. https://doi.org/10.1155/2021/8816250

18. Gogotsi, Y., Penner, R. M., "Energy storage in nanomaterials–capacitive, pseudocapacitive, or battery-like?", *ACS Nano*, Vol. 12, No. 3, (2018), 2081-2083. https://doi.org/10.1021/acsnano.8b01914

19. Conway, B. E., *Electrochemical Supercapacitors: Scientific Fundamentals and Technological Applications*, Springer Science & Business Media, (1999), 698. https://doi.org/10.1007/978-1-4757-3058-6

20. Wang, C., Zhao, Y., Zhai, X., Ding, C., Zhao, X., Li, J., Jin, H., "Graphene boosted pseudocapacitive lithium storage: A case of G-Fe_2O_3", *Electrochimica Acta*, Vol. 282, (2018), 955-963. https://doi.org/10.1016/j.electacta.2018.07.022

21. Wang, K., Li, L., Zhang, T., Liu, Z., "Nitrogen-doped graphene for supercapacitor with long-term electrochemical stability", *Energy*, Vol. 70, (2014), 612-617. https://doi.org/10.1016/j.energy.2014.04.034

22. Wei, W., Ihrfors, C., Björefors, F., Nyholm, L., "Capacity Limiting Effects for Freestanding, Monolithic TiO_2 Nanotube Electrodes with High Mass Loadings", *ACS Applied Energy Materials*, Vol. 3, No. 5, (2020), 4638-4649. https://doi.org/10.1021/acsaem.0c00298

23. Liu, Z., Andreev, Y. G., Armstrong, A. R., Brutti, S., Ren, Y., Bruce, P. G., "Nanostructured TiO_2 (B): the effect of size and shape on anode properties for Li-ion batteries", *Progress in Natural Science: Materials International*, Vol. 23, No. 3, (2013), 235-344. https://doi.org/10.1016/j.pnsc.2013.05.001

24. Zhang, H., Li, G. R., An, L. P., Yan, T. Y., Gao, X. P., Zhu, H. Y., "Electrochemical lithium storage of titanate and titania nanotubes and nanorods", *The Journal of Physical Chemistry C*, Vol. 111, No. 16, (2007), 6143-6148. https://doi.org/10.1021/jp0702595

25. Wang, W., Li, Y., Li, L., Wang, L., Wang, K., "SnO_2/TiO_2 Nanocomposite Prepared by Pulsed Laser Deposition as Anode Material for Flexible Quasi-solid-state Lithium-Ion Batteries", *International Journal of Electrochemical Science*, Vol. 15, No. 12, (2020), 11709-11722. https://doi.org/10.20964/2020.12.49

26. Wei, J., Liu, J. X., Wu, Z. Y., Zhan, Z. L., Shi, J., Xu, K., "Research on the Electrochemical Performance of Rutile and Anatase Composite TiO_2 Nanotube Arrays in Lithium-Ion Batteries", *Journal of Nanoscience and Nanotechnology*, Vol. 15, No. 7, (2015), 5013-5019. https://doi.org/10.1166/jnn.2015.9847

27. Ortiz, G. F., Hanzu, I., Djenizian, T., Lavela, P., Tirado, J. L., Knauth, P., "Alternative Li-Ion Battery Electrode Based on Self-Organized Titania Nanotubes", *Chemistry of Materials*, Vol. 21, No. 1, (2009), 63-67. https://doi.org/10.1021/cm801670u

28. Wang, W., Tian, M., Abdulagatov, A., George, S. M., Lee, Y. C., Yang, R., "Three-dimensional Ni/TiO_2 nanowire network for high areal capacity lithium ion microbattery applications", *Nano Letters*, Vol. 12, No. 2, (2012), 655-660. https://doi.org/10.1021/nl203434g

29. Lou, S., Cheng, X., Gao, J., Li, Q., Wang, L., Cao, Y., Ma, Y., Zuo, P., Gao, Y., Du, C., Huo, H., "Pseudocapacitive Li+ intercalation in porous $Ti_2Nb_{10}O_{29}$ nanospheres enables ultra-fast lithium storage", *Energy Storage Materials*, Vol. 11, (2018), 57-66. https://doi.org/10.1016/j.ensm.2017.09.012

30. Liu, G., Zhao, L., Sun, R., Chen, W., Hu, M., Liu, M., Duan, X., Zhang, T., "Mesoporous $TiNb_2O_7$ microspheres as high performance anode materials for lithium-ion batteries with high-rate capability and long cycle-life", *Electrochimica Acta*, Vol. 259, (2018), 20-27. https://doi.org/10.1016/j.electacta.2017.10.138

31. Liu, S., Zhou, J., Cai, Z., Fang, G., Pan, A., Liang, S., "Nb_2O_5 microstructures: a high-performance anode for lithium ion batteries", *Nanotechnology*, Vol. 27, No. 46, (2016), 46LT01. https://doi.org/10.1088/0957-4484/27/46/46lt01

32. Lübke, M., Shin, J., Marchand, P., Brett, D., Shearing, P., Liu, Z., Darr, J. A., "Highly pseudocapacitive Nb-doped TiO_2 high power anodes for lithium-ion batteries", *Journal of Materials Chemistry A*, Vol. 3, No. 45, (2015), 22908-22914. https://doi.org/10.1039/c5ta07554h

33. Mohammadifar, M., Massoudi, A., Naderi, N., Eshraghi, M. J., "Nb_2O_5 Nanoparticles Synthesis by Chemical Surfactant-Free Methods: ltrasonic Assisted Approach", *Advanced Ceramics Progress*, Vol. 2, No. 4, (2016), 13-17. https://doi.org/10.30501/ACP.2016.90836

34. Regonini, D., Bowen, C. R., Jaroenworaluck, A., Stevens, R., "A review of growth mechanism, structure and crystallinity of anodized TiO_2 nanotubes", *Materials Science and Engineering: R: Reports*, Vol. 74, No. 12, (2013), 377-406. https://doi.org/10.1016/j.mser.2013.10.001

35. Kim, H. Y., Han, J. A., Kweon, D. K., Park, J. D., Lim, S. T., "Effect of ultrasonic treatments on nanoparticle preparation of acid-hydrolyzed waxy maize starch", *Carbohydrate Polymers*, Vol. 93, No. 2, (2013), 582-588. https://doi.org/10.1016/j.carbpol.2012.12.050

36. Sun, L., Li, J., Wang, C., Li, S., Lai, Y., Chen, H., Lin, C., "Ultrasound aided photochemical synthesis of Ag loaded TiO_2 nanotube arrays to enhance photocatalytic activity", *Journal of Hazardous Materials*, Vol. 171, No. 1-3, (2009), 1045-1050. https://doi.org/10.1016/j.jhazmat.2009.06.115

37. Lindström, H., Södergren, S., Solbrand, A., Rensmo, H., Hjelm, J., Hagfeldt, A., Lindquist, S. E., "Li+ Ion Insertion in TiO_2 (Anatase). 2. Voltammetry on Nanoporous Films", *The Journal of Physical Chemistry B*, Vol. 101, No. 39, (1997), 7717-7722. https://doi.org/10.1021/jp970490q

38. Venkatachalam, P., Kesavan, T., Maduraiveeran, G., Kundu, M., Sasidharan, M., "Self-assembled mesoporous Nb_2O_5 as a high performance anode material for rechargeable lithium ion batteries", *Materials Research Express*, Vol. 6, No. 3, (2018), 035502. https://doi.org/10.1088/2053-1591/aaf350